Amorphization Driven by Defect-Induced Mechanical Instability

Chao Jiang,* Ming-Jie Zheng, Dane Morgan,† and Izabela Szlufarska‡
Department of Materials Science and Engineering, University of Wisconsin, Madison, Wisconsin 53706, USA
(Received 27 July 2013; published 7 October 2013)

Using *ab initio* molecular dynamics simulations, we perform a comparative study of the defect accumulation process in silicon carbide (SiC) and zirconium carbide (ZrC). Interestingly, we find that the fcc Si sublattice in SiC spontaneously and gradually collapses following the continuous introduction of C Frenkel pairs (FPs). Above a critical amorphization dose of ~0.33 displacements per atom (dpa), the pair correlation function exhibits no long-range order. In contrast, the fcc Zr sublattice in ZrC remains structurally stable against C sublattice displacements up to the highest dose of 1.0 dpa considered. Consequently, ZrC cannot be amorphized by the accumulation of C FPs. We propose defect-induced mechanical instability as the key mechanism driving the amorphization of SiC under electron irradiation.

DOI: 10.1103/PhysRevLett.111.155501 PACS numbers: 61.80.Az, 61.72.J−

Because of their excellent properties such as high melting temperatures and mechanical strength, cubic silicon carbide (SiC) and zirconium carbide (ZrC) are promising candidates for use as structural and cladding materials in next-generation nuclear reactors [1–4]. For long-term service in nuclear reactors, a material must be highly resistant to irradiation damage. This is because irradiation will create numerous point defects and their complexes, which with time will accumulate and lead to undesired consequences such as crystalline-to-amorphous (*c*-*a*) transition [5]. The zinc blende structure of SiC and the rocksalt structure of ZrC both consist of two interpenetrating face centered cubic (fcc) sublattices, which are occupied by Si (Zr) and C atoms, respectively. Despite their structural similarity, the two materials exhibit vastly different behavior under irradiation. While SiC can be amorphized under electron [6,7], neutron [8], and ion [9] irradiations, no irradiation-induced amorphization of ZrC has been reported to date [10,11]. Those experimental observations are further supported by classical molecular dynamics simulation studies [12–14].

To date, the fundamental mechanisms leading to the *c*-*a* transition under irradiation are still not well understood since these mechanisms are challenging to access experimentally (see Refs. [15,16] for a review). Here, we focus on electron irradiation conditions where irradiation damage involves mostly the accumulation of Frenkel pairs (FPs), i.e., interstitials and vacancies in equal amounts. The amorphization in electron-irradiated materials is often modeled as a transformation that occurs after the cumulative energy of all point defects reaches a critical value, which is equal to the energy difference between the amorphous and crystalline states of a material (ΔE_{am}) [17,18]. Note that this is in contrast to ion-irradiation-induced amorphization, which can occur heterogeneously in a progressive manner, e.g., due to the accumulation of direct in-cascade amorphization [16].

In this Letter, we perform *ab initio* molecular dynamics (AIMD) simulations based on density functional theory (DFT) to bring insights into the electron-irradiation-induced *c*-*a* transition and to provide an atomic-level explanation of the dramatic difference in amorphization resistances between SiC and ZrC. For SiC, a mechanism for amorphization driven by defect-induced mechanical instability is proposed in this work.

In cubic SiC, the average threshold displacement energy (E_d) for the C and Si sublattice was calculated to be 19 and 38 eV, respectively, [19]. In ZrC, the value of E_d for the C and Zr sublattice is 24 and 35 eV, respectively, [20]. Here E_d is defined as the minimum kinetic energy necessary to create a stable FP without spontaneous recombination. In electron irradiation experiments, the maximum recoil energy transferred to an atom (T_{max}) is given by [21]

$$T_{\mathrm{max}} = \frac{2E(E + 2m_0c^2)}{Mc^2}, \tag{1}$$

where E is the incident electron energy, m_0 is the static mass of an electron, M is the mass of the atom, and c is the speed of light. In the experiments of Ishimaru *et al.* [7], an electron energy of 200 keV was used. The corresponding T_{max} values for C, Si, and Zr atoms are 43.7, 18.7, and 5.8 eV, respectively. Under this irradiation condition, only C atoms can be permanently displaced since T_{max} is greater than E_d.

In the present study, we focus on situations where only atomic displacements within the C sublattice occur. Starting from a perfect 216-atom ($3 \times 3 \times 3$) cubic SiC (ZrC) cell with periodic boundary conditions, we simulate the defect accumulation process by repeatedly choosing a C atom at random and then displacing it in an arbitrary direction with a magnitude of $1.0a_0$, which exceeds the spontaneous recombination distances for C FPs in both SiC and ZrC [19,20]. A similar simulation technique has been used in Refs. [13,22–25]. Here, a_0 is the cubic lattice parameter of SiC or ZrC. We require that the displaced C atom be at least 1 Å away from any other atoms in the cell. Between two consecutive displacement events, we allow the cell to relax by performing AIMD simulations at a constant temperature of 100 K for a total duration of 0.5 ps. The time step is 1 fs.

Simulations are performed in a canonical ensemble with the cell volume fixed at that of perfect cubic SiC (ZrC) under zero pressure conditions. For temperature control, velocity rescaling is performed every 50 time steps. Note that the dose rate in our study is around 9×10^9 displacements per atom (dpa) per sec, which is orders of magnitudes faster than that used in experiments. Such an extreme dose rate hinders any defect migration processes in our simulations. However, we expect the dose rate effect to be less important at low temperatures where defect kinetics is sluggish. Indeed, in the electron irradiation experiments [6], the dose to amorphization for SiC is almost constant below 250 K, indicating that defect kinetics does not play an important role at low temperatures. For reference, we have further generated the fully amorphous structures of SiC and ZrC using the liquid-quenching method [26]. Here the SiC (ZrC) system is first equilibrated at 6000 K for 10 ps and then quenched to 100 K over a period of 15 ps, which corresponds to a rapid cooling rate of about 4×10^{14} K/s.

AIMD simulations are performed using the Vienna *ab initio* simulation package (VASP) [27]. For the exchange-correlation functional, we employ the generalized gradient approximation of Perdew, Burke, and Ernzerhof [28]. The electron-ion interactions are described by the projector-augmented wave method [29]. The plane-wave cutoff energy is set at 400 eV. A single Γ point is used to sample the Brillouin zone. By computing the Hellmann-Feynman forces and stress components, we fully relax the unit cell volumes and internal atomic positions of all structures from AIMD simulations using a conjugate gradient scheme.

We judge when a material is fully amorphized under irradiation by monitoring its pair correlation function (PCF) as a function of irradiation dose. For SiC, the critical amorphization dose is found to be ~0.33 dpa, above which the pair correlation function of irradiated SiC is rather similar to that of the amorphous SiC quenched from liquid [Fig. 1(a)]. In contrast, no amorphization of ZrC is observed since long-range order persists up to the highest dose of 1.0 dpa considered in our AIMD simulations [Fig. 1(b)]. Note that for SiC, our predicted critical amorphization dose is somewhat larger than the value (0.2 dpa) predicted by Devanathan *et al.* [13] This discrepancy may be due to the different potential energy surfaces predicted by empirical potentials used by Devanathan *et al.* and by DFT methods used in our study. Furthermore, in electron irradiation experiments, a small fraction (typically ~20% [21]) of the displaced atoms return to their original lattice positions, so that the total number of produced FPs is smaller than the total number of irradiation-induced displacements. Assuming no thermal recovery of irradiation damage, we predict that a dose of around 0.41 dpa is needed in electron irradiation experiments to fully amorphize SiC, which agrees well with the experimentally value of 0.5 dpa [30] measured at 30 K.

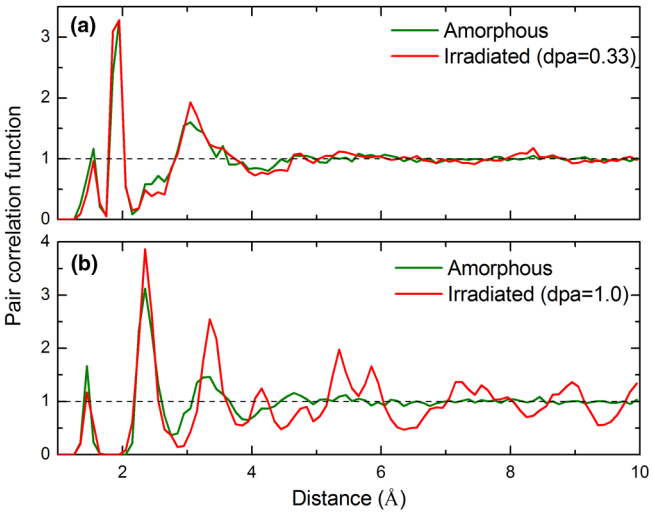

FIG. 1 (color online). Total pair correlation functions of irradiated SiC (a) and ZrC (b) at a dose of 0.33 and 1.0 dpa, respectively. Pair correlation functions of the fully amorphous SiC and ZrC structures obtained from liquid quenching are also shown for comparison.

Figure 2(a) shows the energy of SiC and ZrC as a function of C displacement dose. With increasing dose, the energy of irradiated SiC increases and exceeds that of the amorphous, melt-quenched SiC bulk also around 0.33 dpa. Note that ΔE_{am} of SiC calculated in our study using DFT methods is 0.635 eV/atom, which is in a reasonable agreement with the values (0.6–0.9 eV/atom) obtained from empirical molecular dynamics simulations [13,31]. In contrast, the energy of irradiated ZrC reaches a steady state above ~0.3 dpa and never increases to the energy of that of the fully amorphous state ($\Delta E_{\mathrm{am}} =$ 0.553 eV/atom from the present study). Therefore, results from our thermodynamic analysis are consistent with those from the topological analysis presented in Fig. 1.

To understand what types of point defects contribute to the amorphization of SiC, we plot in Fig. 2(b) the number of point defects in SiC as a function of dose. Here, we identify point defects by analyzing the atom positions in a damaged cell with respect to Voronoi polyhedra centered on ideal lattice sites [32]. Surprisingly, in addition to the C FPs that we introduce, antisite defects (atoms occupying the wrong sublattice) and Si FPs are also generated in large amounts. At 0.33 dpa, C FPs, antisite defects, and Si FPs account for 50%, 36%, and 14% of total defects, respectively. In contrast, in irradiated ZrC, C FPs are the dominating defects ($>$ 94%) with the fractions of other types of point defects being negligibly small [Fig. 2(c)]. Our results thus indicate that SiC and ZrC exhibit fundamentally different atomic-level responses to electron irradiation.

In our AIMD simulations, only C interstitials and C vacancies are introduced, and they are introduced in equal amounts. Here we consider how C FPs can drive formation of other types of defects in SiC using the energetics of isolated point defects from our recent DFT study [33].

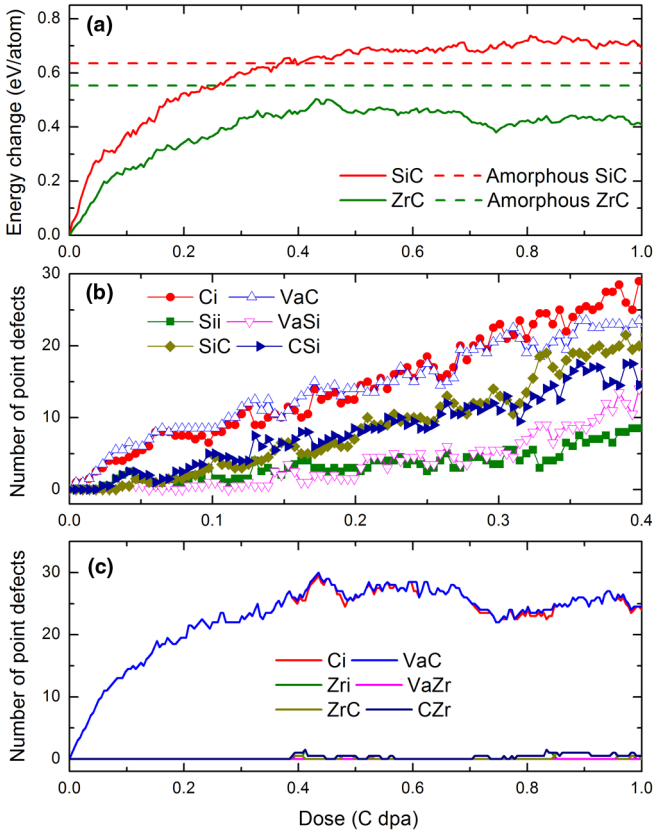

FIG. 2 (color online). (a) The energy change of SiC and ZrC as a function of C displacement dose. For comparison, the energies of amorphous SiC and ZrC are shown as dashed lines. The total number of point defects in SiC and ZrC as a function of irradiation dose are shown in (b) and (c), respectively.

While a C interstitial can displace a lattice Si atom to form a C antisite and a Si interstitial via the reaction $C_i + Si_{Si} \rightarrow C_{Si} + Si_i$, such a reaction is energetically very unfavorable and costs an energy of 5.84 eV. Here, we assume that all defects are in their neutral charge states. Alternatively, a C vacancy can transform into a Si antisite and a Si vacancy by the reaction $Va_C + Si_{Si} \rightarrow Si_C + Va_{Si}$. Again, such a reaction is unlikely since it costs an energy of 7.0 eV. Clearly, in SiC, the formation of a large number of antisite defects and Si FPs due to exclusive C displacements cannot be justified by thermodynamic arguments.

To unravel the origin of this apparent discrepancy, we perform a visual inspection of the atomic structures of irradiated SiC. Interestingly, we find that the fcc Si sublattice is gradually destroyed by the continuous introduction of C FPs. Above a dose of ~0.3 dpa, all the crystalline planes and rows of the Si sublattice are completely lost, indicating full amorphization [Fig. 3(a)]. At lower doses, there exist a mixture of locally amorphous and crystalline domains in SiC [Fig. 3(b)]. In contrast, the fcc Zr sublattice in ZrC remains largely intact even after a large number of displacements within the C sublattice [Fig. 3(c)]. Consistent with our previous DFT study of defect clustering in SiC [34], we find that the displaced C atoms (interstitials) in SiC tend to aggregate into chainlike defect complexes. The clustering tendency of C interstitials is also evident in ZrC. Such strong defect-defect interactions can reduce a significant amount of defect energy, which leads to the nonlinearity of the energy vs dose curves in Fig. 2(a).

For a quantitative analysis of the effects of C FPs on the Si (Zr) sublattices, we define the crystallinity of the fcc Si (Zr) sublattice ($\psi_{Si(Zr)}$) in SiC (ZrC) as the fraction of Si (Zr) atoms whose common neighbor analysis (CNA) patterns [35] match that of the fcc lattice. During CNA analysis, all C atoms are ignored. The cutoff distance is set at $(\sqrt{2} + 2)a_0/4$, i.e., an average of the first and second nearest neighbor distances of the fcc lattice. In fully ordered and fully amorphous SiC (ZrC), $\psi_{Si(Zr)}$ is equal to 1 and 0, respectively. Interestingly, Fig. 4 shows that the Si sublattice in SiC does not suddenly collapse as a whole at a critical C FP concentration. Instead, the Si sublattice gradually loses its crystallinity as the C displacement dose increases. Above a critical dose of ~0.3 dpa, ψ_{Si} becomes essentially zero, indicating full amorphization of SiC. In contrast, the Zr sublattice in ZrC remains crystalline up to high C dpa with the crystallinity measure fluctuating around a constant value of $\psi_{Zr} \sim 0.35$ above about 0.3 dpa. Consequently, accumulation of C FPs alone cannot drive the amorphization of ZrC.

To better understand why the Zr sublattice remains stable under C displacements while the Si sublattice does not, we calculate the phonon spectra of fcc Si and fcc Zr using the direct force-constant approach [36], as implemented in ATAT [37]. Phonon calculations are performed using large 128-atom supercells, which allows the inclusion of long-range force constants in the fitting. The magnitude of atomic displacements is chosen to be 0.2 Å. As can be seen in Fig. 5(a), the fcc Si lattice is mechanically unstable since it exhibits imaginary phonon frequencies (soft modes) at both X and L points. In SiC, the stability of the Si sublattice strongly depends on the C sublattice through the formation of intersublattice Si-C bonds. Consequently, following the damage to the C sublattice by electron irradiation, the Si sublattice will spontaneously collapse, as observed in Fig. 3. This collapse may be related to the tendency of SiC to amorphize. Our results suggest that it is the intrinsic mechanical instability of the Si sublattice that drives the amorphization of SiC under electron irradiation. Note that since the Voronoi analysis is not strictly valid when lattice periodicity is lost, the antisite defects and Si FPs in SiC found by this method (Fig. 2(b) are most likely artifacts due to the collapse of the Si sublattice. In contrast, the fcc Zr structure is mechanically stable since all phonon frequencies are positive throughout the Brillouin zone [Fig. 5(b)]. Because of the intrinsic stability of the fcc Zr sublattice, it can withstand a highly defective C sublattice generated by C displacements, which may explain the superior amorphization resistance of ZrC.

Before closing, it is worthwhile to mention that we have also performed AIMD simulations of exclusive Si

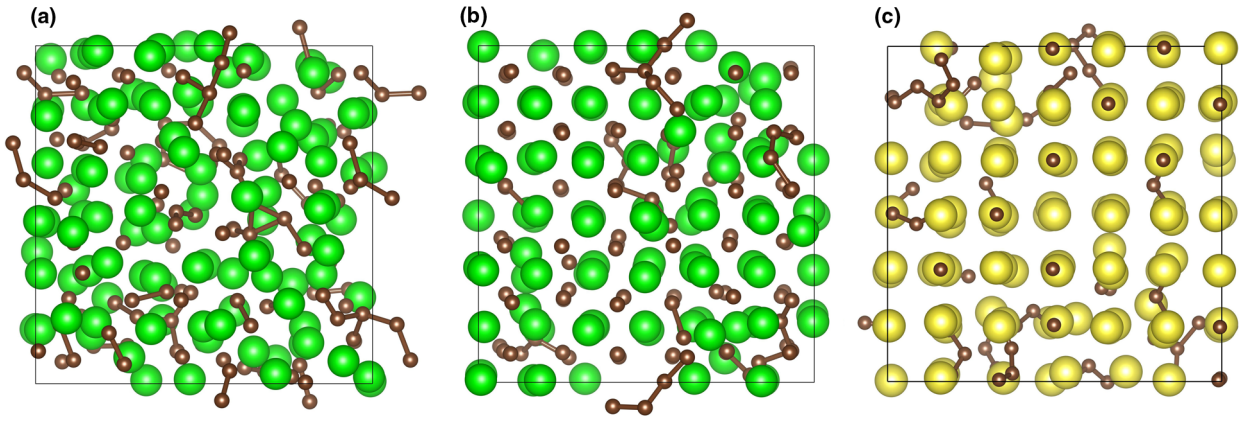

FIG. 3 (color online). Projection of atom positions in irradiated SiC at a dose of (a) 0.33 dpa and (b) 0.16 dpa. (c) Atomic structure of ZrC at a dose of 1.0 dpa. Large and small spheres represent Si (Zr) and C atoms, respectively. All nearest-neighbor homonuclear C-C bonds ($d_{\text{C-C}} < 1.8$ Å) are shown.

sublattice displacements in SiC. We find that most of the displaced Si atoms instantaneously recombine with Si vacancies, consistent with the very low recombination barrier for Si FPs (0.03 eV [38]) in SiC. In comparison, an isolated C interstitial recombines with a C vacancy in SiC with a much higher barrier of 0.90 eV [38]. The strong tendency of C interstitials towards clustering can further hinder their recombination with vacancies. Our simulations thus show that, in the absence of defects within the C sublattice, the Si sublattice in SiC is actually remarkably resistant to irradiation damage. This observation provides further evidence that the collapse of the Si sublattice in SiC is triggered by its intrinsic mechanical instability.

It is also instructive to ask about the role of chemical disorder in amorphization of SiC. For instance, it has been demonstrated by Hobbs and co-workers [39] that accumulation of chemical disorder in SiC can lead to amorphization of this material. Chemical disorder can be quantified as the fraction of homonuclear to heteronuclear bonds $\chi = N_{\text{C-C}}/N_{\text{Si-C}}$, where $N_{i\text{-}j}$ denotes the total number of i-j bonds. To test whether accumulation of chemical disorder is necessary for amorphization of SiC, we perform additional simulations where we only introduce C vacancies. Creation of C vacancies alone does not introduce any homonuclear C-C bonds and we ask whether SiC will amorphize under such conditions. To this end, we randomly remove half of the C atoms from a perfect 216-atom SiC cell and anneal the defective cell at 100 K for 10 ps using AIMD. Consistent with its intrinsic instability, we find that the Si sublattice in SiC collapses following the introduction of C vacancies [40]. The crystallinity of the Si

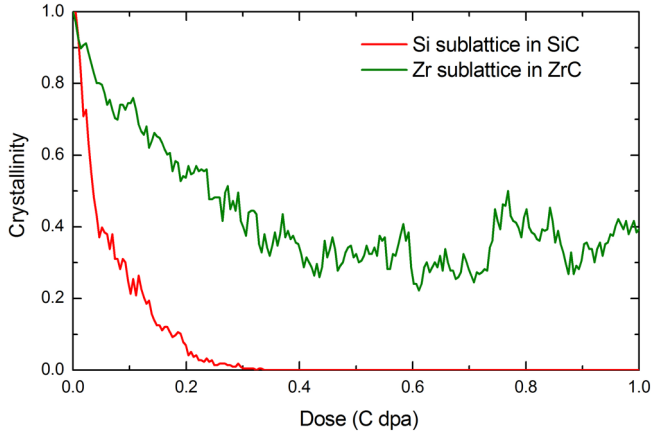

FIG. 4 (color online). Crystallinity $\psi_{\text{Si(Zr)}}$ of the Si and Zr sublattices in SiC and ZrC, respectively, as a function of C displacement dose. Crystallinity $\psi_{\text{Si(Zr)}}$ is defined based on the CNA analysis, as explained in the text. $\psi_{\text{Si(Zr)}} = 1$ corresponds to the case of perfect crystalline order in the entire lattice.

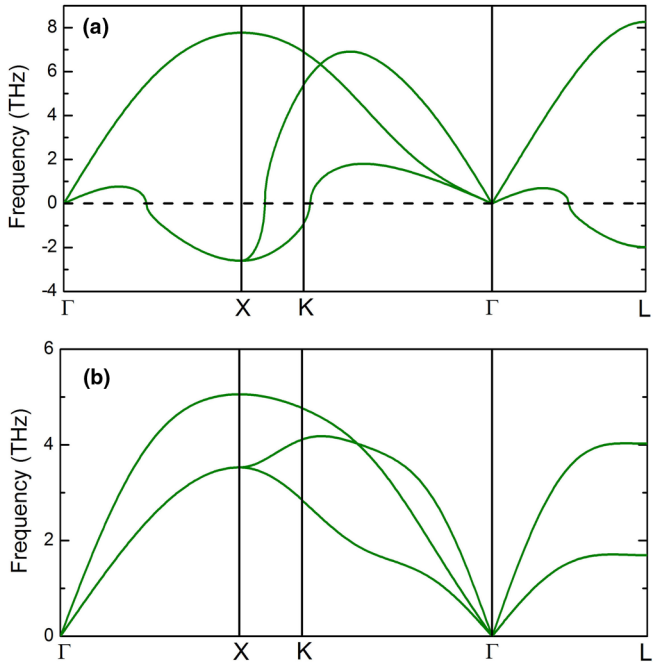

FIG. 5 (color online). Calculated phonon dispersion relations for (a) fcc Si and (b) fcc Zr along various high-symmetry directions in the Brillouin zone.

sublattice is calculated to be only 0.037, very close to that in fully amorphous SiC ($\psi_{Si} = 0$). Our results thus suggest that, while chemical disorder can play an important role in amorphization [39], SiC can be amorphized without prior formation of C-C homonuclear bonds. We have performed similar calculations for ZrC, also removing half the C atoms. As expected, the Zr sublattice can tolerate the vacancies in the C sublattice and remains perfectly crystalline with $\psi_{Zr} = 1.0$ [40].

In summary, we have performed *ab initio* molecular dynamics simulations in an effort to reveal the microscopic origin of the dramatic difference in amorphization resistances between SiC and ZrC. Interestingly, we find that the fcc Si sublattice in SiC spontaneously collapse following the introduction of C Frenkel pairs. In the absence of defects within the C sublattice, the Si sublattice is however highly radiation tolerant due to fast damage recovery. Our results thus indicate defect-induced mechanical instability as a likely mechanism for the amorphization of SiC under electron irradiation. We further demonstrate that the amorphization of SiC is a continuous rather than an abrupt process. In contrast to SiC, the fcc Zr sublattice in ZrC is intrinsically mechanically stable and can tolerate a highly defective C sublattice. Consequently, it is not possible to amorphize ZrC by exclusively displacing C atoms.

This research is supported by U.S. Department of Energy, Office of Basic Energy Sciences Grant No. DE-FG02-08ER46493. This work benefitted from the use of the Extreme Science and Engineering Discovery Environment (XSEDE), which is supported by National Science Foundation Grant No. OCI-1053575.

*Corresponding author.
chaopsu@gmail.com
†Corresponding author.
dmorgan@wisc.edu
‡Corresponding author.
szlufarska@wisc.edu

[1] S. Zinkle and J. Busby, Mater. Today **12**, 12 (2009).
[2] Y. Katoh, L. L. Snead, I. Szlufarska, and W. J. Weber, Curr. Opin. Solid State Mater. Sci. **16**, 143 (2012).
[3] L. L. Snead, Y. Katoh, and S. Kondo, J. Nucl. Mater. **399**, 200 (2010).
[4] S. Kim, I. Szlufarska, and D. Morgan, J. Appl. Phys. **107**, 053521 (2010).
[5] K. E. Sickafus, R. W. Grimes, J. A. Valdez, A. Cleave, M. Tang, M. Ishimaru, S. M. Corish, C. R. Stanek, and B. P. Uberuaga, Nat. Mater. **6**, 217 (2007).
[6] H. Inui, H. Mori, A. Suzuki, and H. Fujita, Philos. Mag. B **65**, 1 (1992).
[7] M. Ishimaru, I. T. Bae, and Y. Hirotsu, Phys. Rev. B **68**, 144102 (2003).
[8] L. L. Snead and J. C. Hay, J. Nucl. Mater. **273**, 213 (1999).
[9] W. J. Weber and L. M. Wang, Nucl. Instrum. Methods Phys. Res., Sect. B **106**, 298 (1995).
[10] Y. Yang, C. A. Dickerson, H. Swoboda, B. Miller, and T. R. Allen, J. Nucl. Mater. **378**, 341 (2008).
[11] D. Gosset, M. Dolle, D. Simeone, G. Baldinozzi, and L. Thome, Nucl. Instrum. Methods Phys. Res., Sect. B **266**, 2801 (2008).
[12] F. Gao, W. J. Weber, and R. Devanathan, Nucl. Instrum. Methods Phys. Res., Sect. B **191**, 487 (2002).
[13] R. Devanathan, F. Gao, and W. J. Weber, Appl. Phys. Lett. **84**, 3909 (2004).
[14] L. Van Brutzel and J. P. Crocombette, Nucl. Instrum. Methods Phys. Res., Sect. B **255**, 141 (2007).
[15] H. Inui, H. Mori, and H. Fujita, Acta Metall. **37**, 1337 (1989).
[16] W. J. Weber, Nucl. Instrum. Methods Phys. Res., Sect. B **166–167**, 98 (2000).
[17] A. T. Motta and D. R. Olander, Acta Metall. Mater. **38**, 2175 (1990).
[18] N. Swaminathan, D. Morgan, and I. Szlufarska, J. Nucl. Mater. **414**, 431 (2011).
[19] G. Lucas and L. Pizzagalli, Phys. Rev. B **72**, 161202 (2005).
[20] M. J. Zheng, N. Swaminathan, D. Morgan, and I. Szlufarska (unpublished).
[21] G. S. Was, *Fundamentals of Radiation Materials Science: Metals and Alloys* (Springer, New York, 2007).
[22] H. Hsieh and S. Yip, Phys. Rev. Lett. **59**, 2760 (1987).
[23] A. Chartier, C. Meis, J. P. Crocombette, W. J. Weber, and L. R. Corrales, Phys. Rev. Lett. **94**, 025505 (2005).
[24] A. Chartier, G. Catillon, and J. P. Crocombette, Phys. Rev. Lett. **102**, 155503 (2009).
[25] R. Devanathan, W. J. Weber, and J. D. Gale, Energy Environ. Sci. **3**, 1551 (2010).
[26] F. Finocchi, G. Galli, M. Parrinello, and C. M. Bertoni, Phys. Rev. Lett. **68**, 3044 (1992).
[27] G. Kresse and J. Furthmuller, Phys. Rev. B **54**, 11 169 (1996).
[28] J. P. Perdew, K. Burke, and M. Ernzerhof, Phys. Rev. Lett. **77**, 3865 (1996).
[29] G. Kresse and D. Joubert, Phys. Rev. B **59**, 1758 (1999).
[30] H. Inui, H. Mori, A. Suzuki, and H. Fujita, Philos. Mag. B **66**, 737 (1992).
[31] M. Mishra and I. Szlufarska, Acta Mater. **57**, 6156 (2009).
[32] N. Swaminathan, P. J. Kamenski, D. Morgan, and I. Szlufarska, Acta Mater. **58**, 2843 (2010).
[33] D. Shrader, S. M. Khalil, T. Gerczak, T. R. Allen, A. J. Heim, I. Szlufarska, and D. Morgan, J. Nucl. Mater. **408**, 257 (2011).
[34] C. Jiang, D. Morgan, and I. Szlufarska, Phys. Rev. B **86**, 144118 (2012).
[35] D. Faken and H. Jonsson, Comput. Mater. Sci. **2**, 279 (1994).
[36] K. Parlinski, Z.-Q. Li, and Y. Kawazoe, Phys. Rev. Lett. **78**, 4063 (1997).
[37] A. van de Walle, M. Asta, and G. Ceder, CALPHAD: Comput. Coupling Phase Diagrams Thermochem. **26**, 539 (2002).
[38] M. J. Zheng, N. Swaminathan, D. Morgan, and I. Szlufarska, Phys. Rev. B **88**, 054105 (2013).
[39] X. Yuan and L. W. Hobbs, Nucl. Instrum. Methods Phys. Res., Sect. B **191**, 74 (2002).
[40] See Supplemental Material at http://link.aps.org/supplemental/10.1103/PhysRevLett.111.155501 for the atomic structures of SiC and ZrC after randomly removing half of the C atoms.